ACS Catalysis

pubs.acs.org/acscatalysis

Research Article

Scope and Mechanistic Studies on the Ruthenium-Catalyzed Multicomponent Deaminative C−H Coupling Reaction of Phenols with Aldehydes and Enamines for the Formation of Xanthene and Dioxacyclic Derivatives

Nuwan Pannilawithana,[‖] Mina Son,[‖] Donghun Hwang, Mu-Hyun Baik,* and Chae S. Yi*

Cite This: *ACS Catal.* 2023, 13, 9051−9063

Read Online

ACCESS | Metrics & More | Article Recommendations | Supporting Information

ABSTRACT: The *in situ* generated catalytic system from the tetranuclear Ru−H complex $[(PCy_3)(CO)RuH]_4(O)(OH)_2$ (**1**) with 3,4,5,6-tetrachloro-1,2-benzoquinone (**L1**) has been found to mediate a multicomponent deaminative coupling reaction of phenols with aldehydes and enamines to form xanthene products. The multicomponent C−H coupling reaction of phenols with 2-hydroxybenzaldehydes and cyclic enamines efficiently installed the tricyclic 1,3-dioxacin derivatives, while the analogous coupling reaction of phenols with 2-hydroxybenzaldehydes and triethylamine selectively formed bicyclic 1,5-dioxacyclic derivatives. The density functional theory (DFT) calculations established two energetically viable mechanistic pathways for the formation of xanthene products, in which both pathways identified the C−O bond cleavage step as the turnover limiting step. A Hammett plot from the coupling reaction of 3,5-dimethoxyphenol with an enamine and *para*-substituted benzaldehydes *p*-X-C_6H_4CHO (X = OMe, Me, H, Cl, CF_3) showed a negative slope ($\rho = -0.98$). The calculated energy analysis showed a similar trend ($\rho = -0.59$) for the mechanism via the C−O cleavage rate-limiting step. The combined experimental and DFT computational results support a mechanistic path that involves the dehydrative C−H coupling of phenol with aldehyde, followed by the deaminative coupling reaction with an enamine in forming the xanthene product.

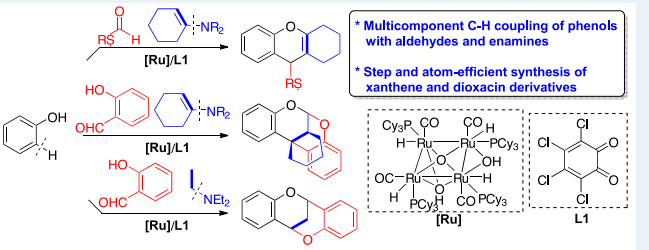

KEYWORDS: *multicomponent reaction, deaminative coupling, ruthenium catalyst, xanthene, dioxacin*

INTRODUCTION

Transition-metal-catalyzed coupling methods via C−N cleavage have emerged as a highly versatile C−C bond formation strategy for the synthesis of complex organic molecules as well as for reforming processes of nitrogen-containing biomass feedstocks.[1] Since simple amines are readily available from a variety of biomass-derived sources,[2] they are highly attractive substrates for the deaminative C−C coupling reactions where the formation of ammonia or amine byproducts would serve as the driving force. Katritzky pyridinium salts, which are readily generated from the reaction of primary amines with pyrylium ion, have been found to be particularly effective reagents for a variety of deaminative cross-coupling reactions under both thermal and photocatalytic conditions.[3] Watson and Martin groups successfully devised highly regioselective Ni-catalyzed deaminative alkylation of unactivated olefins by using pyridinium reagents.[4] Pan and co-workers also reported an efficient Ni-catalyzed deaminative cross-electrophilic coupling reaction of Katritzky salts with alkyl and aryl halides, and later applied to reductive electrochemical coupling with fluorinated olefins.[5] Pyridinium salts have also been extensively used for a number of highly efficient deaminative coupling reactions by using visible-light photoredox catalysis methods.[6] Notably, Fu and co-workers reported an efficient photocatalytic deaminative and decarboxylative alkylation of silyl enol ethers with redox-active esters and *N*-alkylpyridinium salts.[7] The Shang group recently reported a highly enantioselective Ni-catalyzed deaminative alkylation of pyridinium salts of amino acid derivatives with unactivated olefins.[8]

In contrast to pyridinium salts, efforts to devise selective deaminative coupling methods using unactivated amines have long been hampered in part due to a relatively high C−N bond energy and their tendency for undergoing side reactions as well as catalyst poisoning effects.[9] Despite such inherent challeges, a growing number of catalytic deaminative coupling methods have been developed recently by using simple amines.[10] In a seminal work, the Zhang group reported Pd-catalyzed allylic

Received: April 12, 2023
Revised: June 10, 2023
Published: June 23, 2023

alkylation of carbonyl compounds with allylamines, which has been shown to involve a direct allylic C−N bond cleavage via the formation of Pd-allyl species.[11] More recently, Rovis and co-workers developed a highly efficient deaminative alkylation method via C−N bond activation of sterically hindered primary amines by employing dual Ni/photoredox-catalysis.[12]

Concerted research efforts have been devoted to develop multicomponent catalytic C−H coupling methods as a step- and atom-efficient synthetic strategy for assembling complex organic molecules from using readily available hydrocarbon substrates.[13] In a seminal work, Ellman and co-workers devised multicomponent Rh-catalyzed C−H alkenylation and electrocyclization cascade reactions of α,β-unsaturated imines with alkyne substrates to form dihydropyridines and used these as versatile intermediates for synthesizing a variety of nitrogen heterocycles.[14] Balaraman and co-workers developed a tandem synthesis of quinolines via Rh-catalyzed C−H activation of anilines and alkynes with CO surrogates to form quinoline derivatives.[15] The Liang group reported Ru-catalyzed *meta*-selective C−H coupling reaction of arenes with alkenes and fluoroalkyl halides.[16] A number of multicomponent C−H annulation methods have also been devised by using olefins and arene substrates to synthesize both carbocyclic as well as heterocyclic derivatives.[17] Cramer and co-workers devised a highly enantioselective three-component C−H functionalization method of readily available arenes with unsaturated carbonyl compounds to access substituted β-hydroxyketones by using Co(III) catalysts bearing a chiral cyclopentadienyl group.[18] Recently, a number of multicomponent alkene functionalization methods have been achieved by combining nickel catalysis with a photoredox hydrogen atom transfer process.[19]

Our research group has been pursuing the development of new deaminative C−C coupling methods, which utilize readily available simple amine substrates and are driven by the formation of ammonia. We previously discovered that both the tetranuclear Ru−H complex $[(PCy_3)(CO)RuH]_4(\mu\text{-}O)(\mu\text{-}OH)_2$ (**1**) and the cationic Ru−H complex $[(\eta^6\text{-}C_6H_6)(PCy_3)(CO)RuH]^+BF_4^-$ (**2**) with a redox-active 3,4,5,6-tetrachloro-1,2-benzoquinone (**L1**) exhibited uniquely high catalytic activity for the deaminative coupling reactions of ketones with simple amines to form α-alkylated ketone products.[20] We also devised a highly efficient dehydrative C−H coupling reaction of phenols with carbonyl compounds to synthesize oxygen heterocyclic core structures by using the same catalytic system **1**/**L1**.[21] We reasoned that merging these two C−H coupling and deaminative coupling methods might lead to a step-efficient synthetic strategy for a variety of heterocyclic compounds. In this Article, we delineate the scope and synthetic utility of the multicomponent C−H coupling method of phenols with aldehydes and amines as a step-efficient protocol to synthesize both xanthene and dioxacin oxygen heterocycles. We also present the combined experimental and computational studies for elucidating the detailed mechanism of the catalytic coupling method. From both synthetic and environmental points of view, the salient features of the catalytic method are that biologically significant oxygen heterocyclic core structures are efficiently constructed from the multicomponent C−H coupling reaction of readily available phenols with aldehydes and enamines in a highly regio- and stereoselective fashion without employing any reactive reagents or forming wasteful byproducts.

RESULTS AND DISCUSSION

Reaction Discovery and Optimization Study. At the onset of our efforts to devise new catalytic multicomponent coupling methods, we have been exploring the C−H coupling reactions of arenes with a variety of amines and carbonyl compounds. We initially discovered that the catalytic system consisting of the tetranuclear Ru−H complex **1** with a redox-active 3,4,5,6-tetrachloro-1,2-benzoquinone (**L1**) is highly effective for promoting the multicomponent deaminative coupling reaction of 3,5-dimethoxyphenol with benzaldehyde and 4-(1-cyclohexene-1-yl)morpholine to form the 9-substituted xanthene product **3a** (eq 1). The extensive ligand screening procedures established that catalytic system **1**/**L1** exhibits the highest catalytic activity for the coupling reaction among screened Ru catalysts (Table 1).

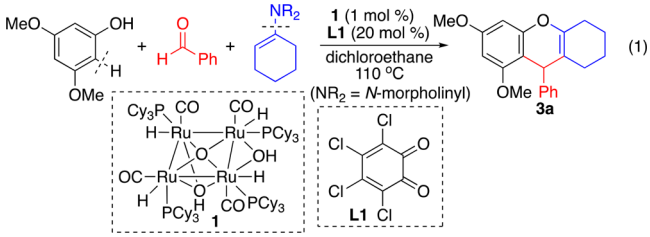

(1)

The cationic Ru−H complexes **2** and $[(PCy_3)_2(CO)(CH_3CN)_2RuH]^+BF_4^-$ also exhibited respectable activity when they are combined with the benzoquinone **L1** (entries 8, 10). It is noteworthy that the presynthesized Ru-catecholate complex **4** was found to exhibit a high catalytic activity without **L1** (entry 9). Other additives such as a hydrogen donor, CO,

Table 1. Catalyst Screening and Optimization Study for the Reaction of 3,5-Dimethoxyphenol with Benzaldehyde and 4-(1-Cyclohexene-1-yl)morpholine

entry	catalyst	deviation from the standard conditions[a]	**3a** (%)[b]
1	**1**	none	76
2	**1**	without **L1**	49
3	**1**	CO (1 atm)	65
4	**1**	2-propanol (1 equiv)	34
5	**1**	3,3-dimethyl-1-butene (1 equiv)	16
6	**1**	in 1,4-dioxane	37
7	**1**	in toluene	11
8	$[(C_6H_6)(PCy_3)(CO)RuH]^+BF_4^-$ (**2**)		68
9	$[(PCy_3)_2(CO)Ru(O\text{-}O)]$ (**4**)[c]	without **L1**	52
10	$[(PCy_3)_2(CO)(CH_3CN)_2RuH]^+BF_4^-$		55
11	$(PCy_3)_2(CO)RuHCl$		31
12	$(p\text{-cymene})RuCl_2$		35
13	$(PPh_3)_3RuCl_2$		26
14	$Ru_3(CO)_{12}$		8
15	$[(COD)RuCl_2]_x$		5
16		**L1** only	0

[a]Standard reaction conditions: 3,5-dimethoxyphenol (0.50 mmol), benzaldehyde (0.50 mmol), 4-(1-cyclohexene-1-yl)morpholine (0.50 mmol), **1** (1 mol %; 4 Ru mol %), **L1** (20 mol %), 1,2-dichloroethane (1 mL), 110 °C, 12 h. [b]The product yield was determined by GC-MS using hexamethylbenzene as an internal standard. **L1** = 3,4,5,6-tetrachloro-1,2-benzoquinone. [c]O-O = 3,5-di-*tert*-butyl-1,2-catecholate.

https://doi.org/10.1021/acscatal.3c01651
ACS Catal. 2023, 13, 9051−9063

Table 2. Multicomponent Deaminative C−H Coupling Reaction of Phenols with Aldehydes and Enamines[a]

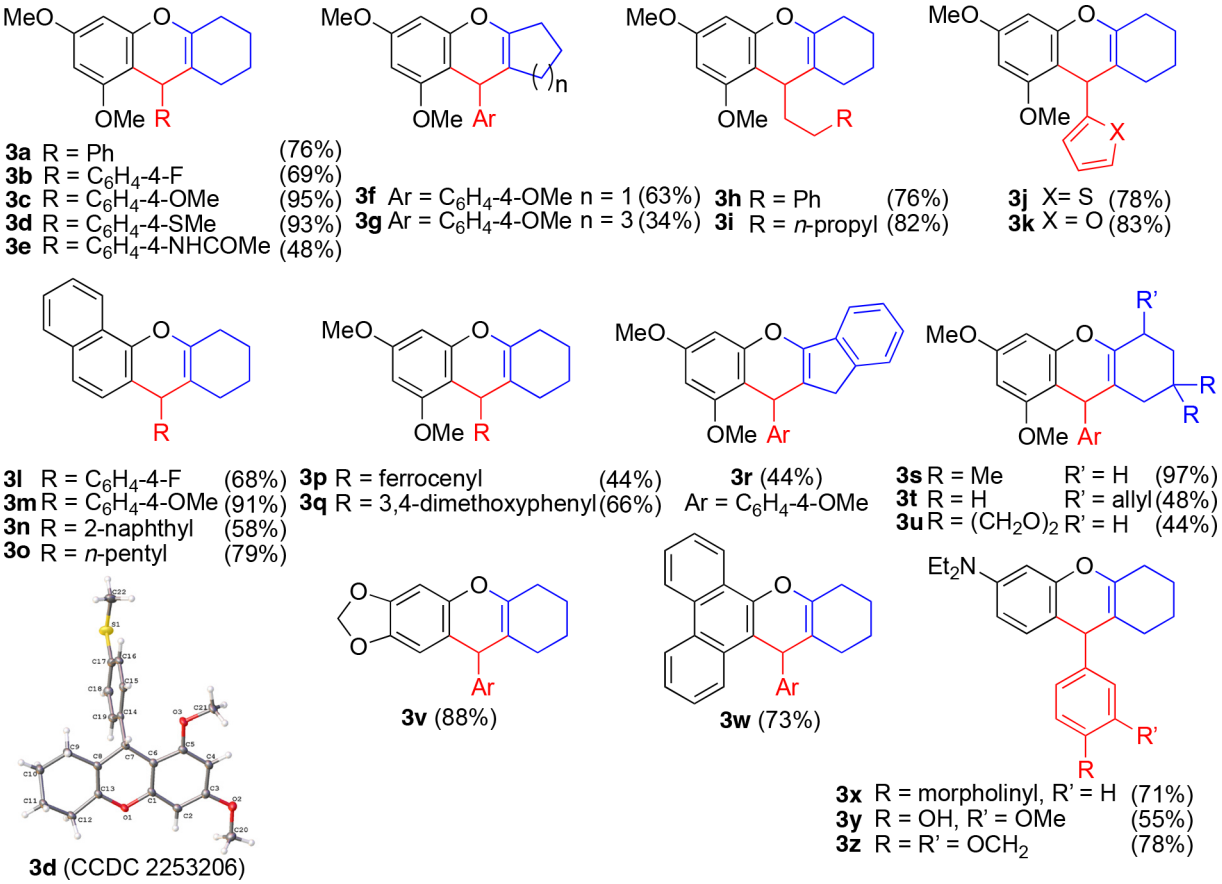

[a]Reaction conditions: phenol (0.5 mmol), aldehyde (0.5 mmol), *N*-morpholinylenamine (0.5 mmol), **1** (1 mol %), **L1** (20 mol %), 1,2-dichloroethane (1 mL), 110 °C, 12 h. Ar = 4-methoxyphenyl.

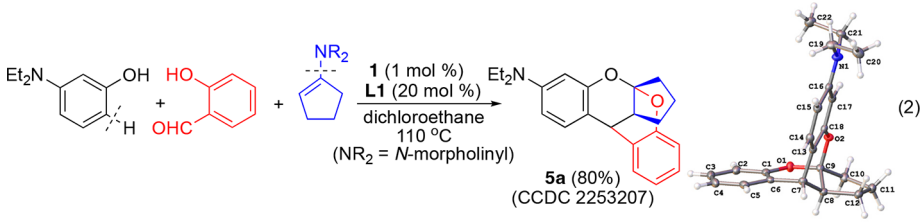

or an olefin were found to be completely ineffective in promoting the coupling reaction (entries 3−5). We subsequently established the standard conditions for the coupling reaction using the tetranuclear Ru−H complex **1** with the benzoquinone **L1**, where 1,2-dichloroethane was found to be the most suitable solvent among screened organic solvents (Tables S1 and S2, Supporting Information). The enamine substrate can be conveniently generated *in situ* from the initial reaction of benzaldehyde with morpholine, which allowed us to carry out a four-component coupling reaction under a one-pot procedure without sacrificing the product yield.

Reaction Scope. The substrate scope of the multicomponent coupling reaction was explored by using the standard conditions (Table 2). Electron-rich phenols such as 3,5-dimethoxyphenol, 3-(diethylamino)phenol, and naphthol derivatives were found to be suitable substrates for the coupling with *para*-substituted benzaldehydes and 4-(1-cyclohexen-1-yl)morpholine to form the xanthene products **3a-e**. The analogous coupling reaction with 4-(1-cyclopentenyl-1-yl)morpholine and 4-(1-cyclohepten-1-yl)morpholine enamines led to the corresponding five- and seven-membered chromene derivatives **3f,g**. The coupling with aliphatic aldehydes as well as with naturally available furfural and heteroarene aldehydes predictively afforded 9-substituted xanthene products **3h,i** and **3j,k**, respectively. Moreover, 1-naphthol smoothly reacted with both aryl-substituted and aliphatic aldehydes to yield xanthene products **3l-o**. A variety of naturally available and highly functionalized aldehydes such as 4-morpholinobenzaldehyde, vanillin, veratraldehyde, and piperonal smoothly reacted with 3-(diethyl)aminophenol and 4-(1-cyclohexene-1-yl)morpholine to yield the anticipated coupling products **3x**, **3y**, **3q**, and **3z**, respectively. The ferrocene-containing carboxaldehyde readily reacted with 3,5-dimethoxyphenol and 4-(1-cyclohexen-1-yl)morpholine to afford the corresponding 9-substituted xanthene product **3p**. The coupling of a number of naturally occurring phenols such as sesamol and polyaromatic 9-phenanthrol smoothly formed xanthene products **3v** and **3w**, respectively. These coupling

https://doi.org/10.1021/acscatal.3c01651
ACS Catal. 2023, 13, 9051−9063

Table 3. Multicomponent Deaminative C−H Coupling Reaction of Phenols with 2-Hydroxybenzaldehydes and Enamines[a]

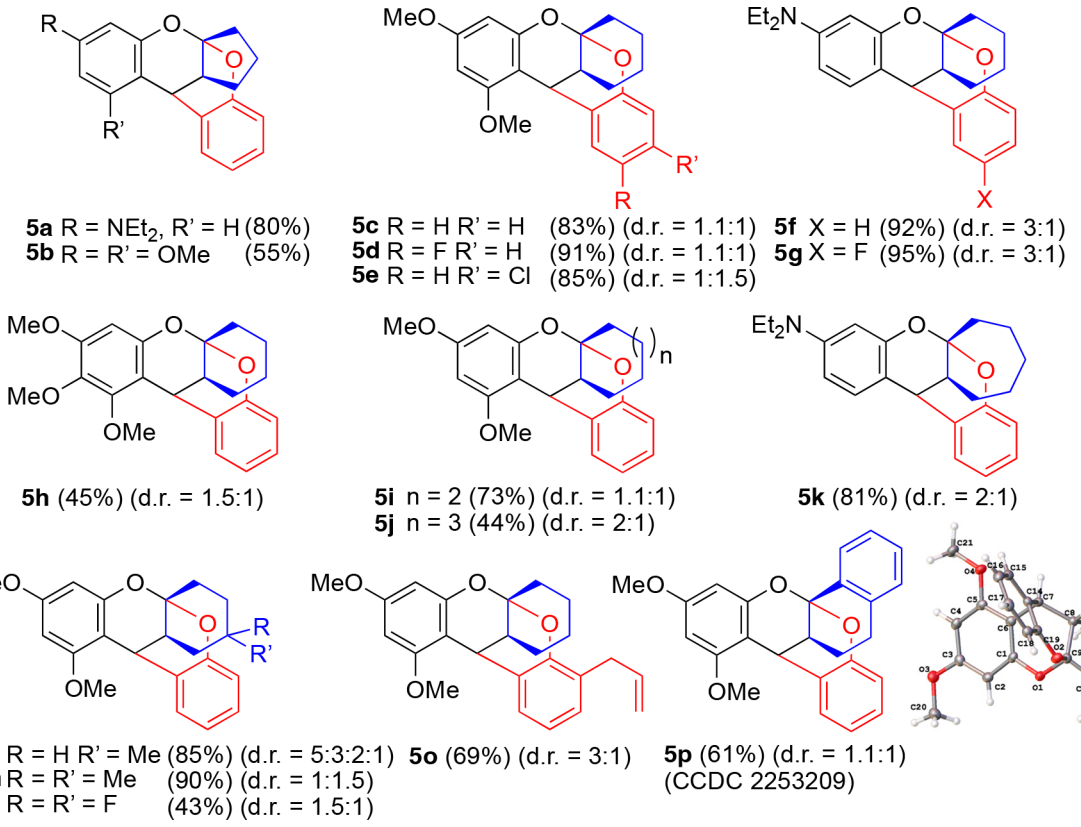

[a]Reaction conditions: phenol (0.5 mmol), aldehyde (0.5 mmol), enamine (0.5 mmol), **1** (1 mol %), **L1** (20 mol %), 1,2-dichloroethane (1 mL), 110 °C, 12 h.

products were readily isolated by column chromatography on silica gel, and their structures were completely established by spectroscopic methods. The molecular structure of **3d** was also determined by X-ray crystallography.

To extend the substrate scope of the multicomponent coupling method, we next explored the coupling reaction of phenols with a variety of functionalized aldehydes and enamines. Thus, the treatment of 3-(diethylamino)phenol with 2-hydroxybenzaldehyde and 4-(1-cyclopentenyl-1-yl)-morpholine in the presence of **1**/**L1** under the standard conditions as established in Table 1 selectively formed the tricyclic 1,3-dioxacin product **5a** in 80% yield (diastereomeric ratio (d.r.) = 10:1) (eq 2). The major diastereomer of **5a** was isolated by silica gel column chromatography, and the 1,3-dioxocin structure of **5a** was initially established using two-dimensional (2D) NMR techniques. The molecular structure of **5a**, which was subsequently determined by X-ray crystallography, confirmed its tricyclic 1,3-dioxacin configuration.

We surveyed the substrate scope of the coupling reaction by using the standard conditions (Table 3). Electron-rich phenol substrates such as 3,5-dimethoxyphenol and 3-(diethylamino)-phenol smoothly reacted with 2-hydroxybenzaldehyde and 4-(1-cyclopentenyl-1-yl)morpholine to form products **5a**,**b**. The coupling reaction of 3,5-dimethoxyphenol with aryl-substituted aldehydes and 4-(1-cyclohexene-1-yl)morpholine formed the expected products **5c**-**e** in a nearly equal diastereomeric ratio (d.r. = 1.1−1.5:1), while the analogous reaction with 3-(diethylamino)phenol generated a 3:1 diastereomeric mixture for both products **5f** and **5g** with an excellent chemical yield. The coupling reaction of electron-rich phenols with 4-(1-cyclohpten-1-yl)morpholine and 4-(1-cycloocten-1-yl)-morpholine enamines led to the corresponding seven- and eight-membered tricyclic 1,3-dioxacin products, **5i** (d.r. = 1.1:1), **5j** (d.r. = 2:1), and **5k** (d.r. = 2:1), respectively. The coupling of 3,5-dimethoxyphenol with 4-substituted cyclic enamines such as 4-(4,4-dimethylcyclohex-1-en-1-yl)-morpholine afforded a 5:3:2:1 diastereomeric mixture of the products **5l**, while the coupling with an allyl-substituted salicylaldehyde formed a 3:1 diastereomeric mixture of **5o**. Interestingly, the coupling reaction of 3,5-dimethoxyphenol with the enamine formed from the reaction of morpholine and α-tetralone also smoothly formed a 1.1:1 diastereomeric mixture of the tricyclic products **5p** in a highly regioselective fashion. The molecular structures of **5a**, **5d**, and **5p** were determined by X-ray crystallography.

The stereochemical assignment of these tricyclic 1,3-dioxacin products was carried out by correlating NMR spectroscopic data with X-ray crystallographic analyses. The major and minor diastereomers of **5a**, **5d**, and **5p** have been successfully separated by silica gel column chromatography, and as stated above, the molecular structures for both the major diastereomers of **5a** and **5p** and the minor diastereomer of **5d** have been unambiguously determined by X-ray crystallography (Figures S3 and S4, Supporting Information). The X-ray crystallographic analysis of the major diastereomers of **5a** and **5p** revealed the configurations on C7(*R*), C8(*S*), and C9(*S*), with overall an *anti*-configuration between the cyclohexyl and the aldehyde benzene groups, probably to minimize the steric interaction between the two groups. In

https://doi.org/10.1021/acscatal.3c01651
ACS Catal. 2023, 13, 9051−9063

Table 4. Multicomponent Deaminative C−H Coupling Reaction of Phenols with 2-Hydroxybenzaldehydes and Triethylamine[a]

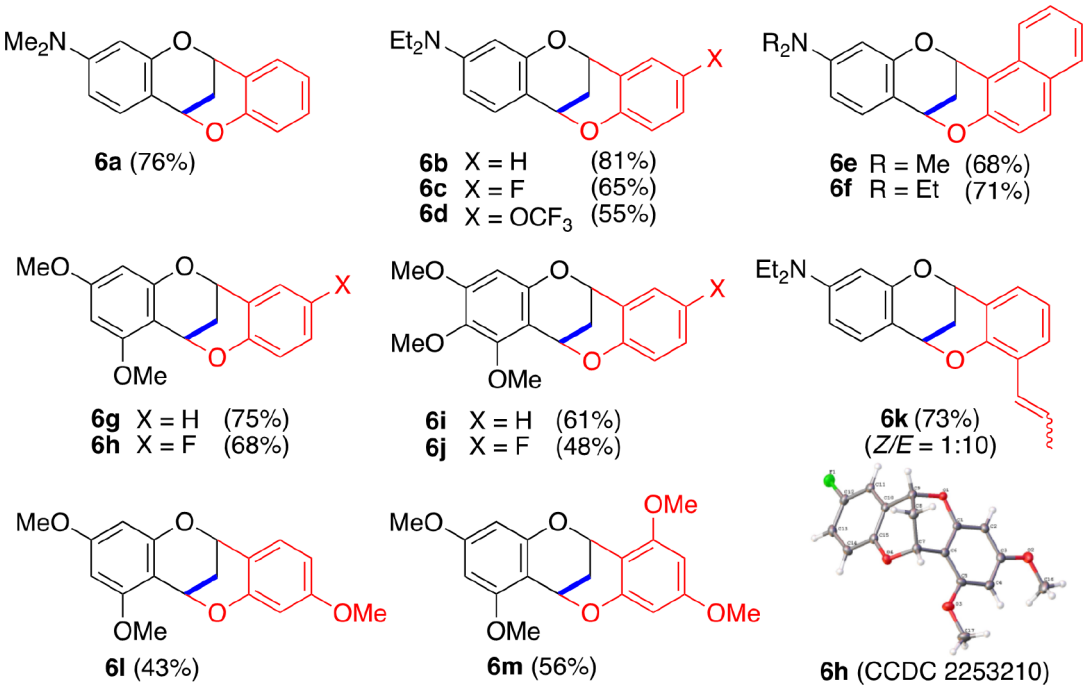

[a]Reaction conditions: phenol (0.5 mmol), aldehyde (0.5 mmol), triethylamine (0.5 mmol), **1** (1 mol %), **L1** (20 mol %), 1,2-dichloroethane (1 mL), 110 °C, 12 h.

contrast, the minor diastereomer of **5d**, which was separated from a 1.1:1 diastereomeric mixture by silica gel column chromatography, has the configurations at C7(*R*), C8(*R*), and C9(*S*) with a *syn*-configuration between the cyclohexyl and the aldehyde benzene rings located on the C8-C9 bond (see Figure S3 in Supporting Information for numbering scheme and stereochemical assignment for both diastereomers). By inferring NMR spectroscopic data from the configurations determined from X-ray crystallographic analysis, we have been able to assign the relative stereochemistry of both diastereomers for **5a**, **5d**, and **5p**.

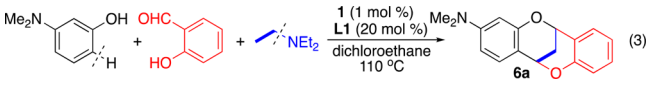

Recognizing that saturated amines would form enamine substrates via the initial dehydrogenation under the reaction conditions,[22] we next sought to explore the suitability of a variety of saturated amines as an "olefin synthon" for the deaminative coupling reaction. Gratifyingly, we found that a readily available tertiary amine, triethylamine, is a suitable substrate for the multicomponent deaminative coupling reaction. Thus, the treatment of 3-(diethylamino)phenol (0.50 mmol) with 2-hydroxybenzaldehyde (0.50 mmol) and triethylamine (0.50 mmol) under otherwise standard conditions smoothly formed the bicyclic 1,5-dioxacin product **6a** (eq 3). An initial survey of saturated amines for the coupling reaction showed that tertiary amines such as *N*,*N*-diethylmethylamine, 1-ethylpiperidine, and 1-ethylpyrrolidine as well as triethylenediamine reacted smoothly to form the product **6a** (Tables S4 and S5, Supporting Information). The coupling reaction with 2-diethylaminoethylamine and *N*,*N*′-diethylethylenediamine also afforded the same product **6a** in moderate to high yields. We also tested the suitability of 1-vinylpyrrolidine as the enamine reagent for the coupling reaction, in which case product **6a** was formed in 81% yield. Unfortunately, other tertiary amines with a longer alkyl chain such as tri-*n*-propylamine and tri-*n*-butylamine were found to be much less effective in promoting the coupling reaction, giving less than 20% yield of the coupling products, and we attribute such low activity of these amine substrates to relative difficulty in generating the enamines.

We surveyed the substrate scope of the multicomponent deaminative coupling reaction using triethylamine as the amine substrate (Table 4). In general, electron-rich phenols such as 3,5-dimethoxyphenol and 3-(dimethylamino)phenol were found to be suitable substrates for the coupling reaction with salicylaldehyde and triethylamine to exclusively form bicyclic 1,5-dioxacin products **6** without any trace of 1,3-dioxacin regioisomers. The coupling of 3-(dimethylamino)phenol with 2-hydroxybenzaldehyde and triethylamine predictively formed the products **6a-d**, while the analogous coupling with 2-hydroxy-1-naphthaldehyde afforded **6e**,**f** in good yields. 2-Hydroxybenzaldehydes bearing an electron-withdrawing group were successfully utilized for the deaminative coupling reaction with 3,5-dimethoxyphenol and 3,4,5-trimethoxyphenol in forming the products **6g-j**. The coupling reaction of 3-(diethylamino)phenol with 3-allylsalicylaldehyde and triethylamine proceeded smoothly, in which the 3-allyl group was isomerized to give 1:10 *Z*/*E* isomers of the product **6k**. The coupling with a dimethoxy-substituted salicylaldehyde also formed product **6m**. The coupling products were readily isolated by column chromatography on silica gel, and their structure was completely established by spectroscopic methods. The structure of **6h** was also determined by X-ray crystallography (Figure S9, Supporting Information). A salient feature of the catalytic method is that a readily available triethylamine has been successfully utilized as an olefin

https://doi.org/10.1021/acscatal.3c01651
ACS Catal. 2023, 13, 9051−9063

Table 5. Multicomponent Deaminative Coupling Reaction of Phenols with Aldehydes and Steroidal Enamines[a]

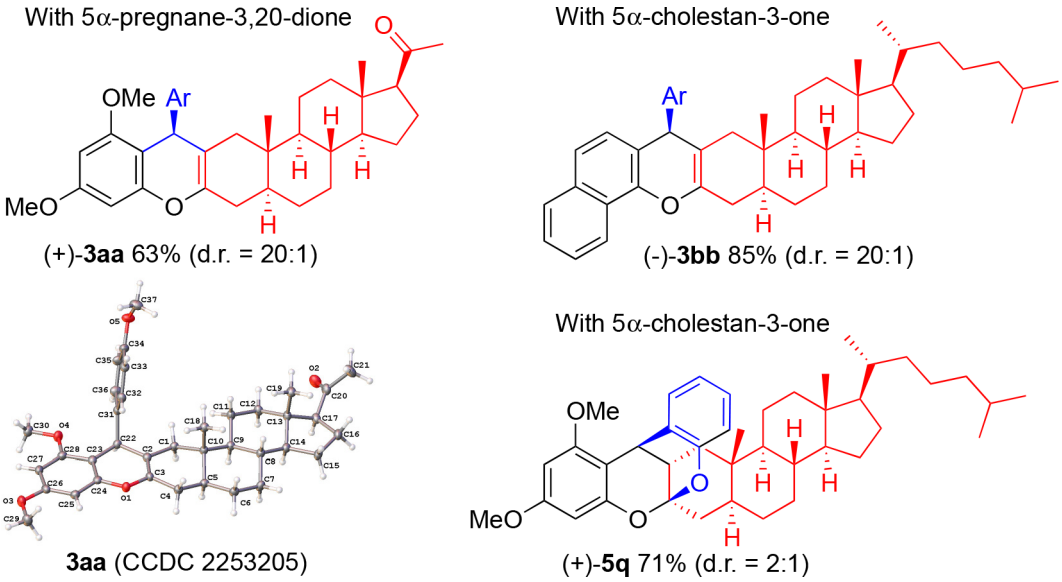

[a]Reaction conditions: phenol (0.50 mmol), aldehyde (0.50 mmol), ketone (0.50 mmol), morpholine (0.5 mmol), **1** (1 mol %), **L1** (20 mol %), 1,2-dichloroethane (1 mL), 110 °C, 12 h. Ar = 4-methoxyphenyl.

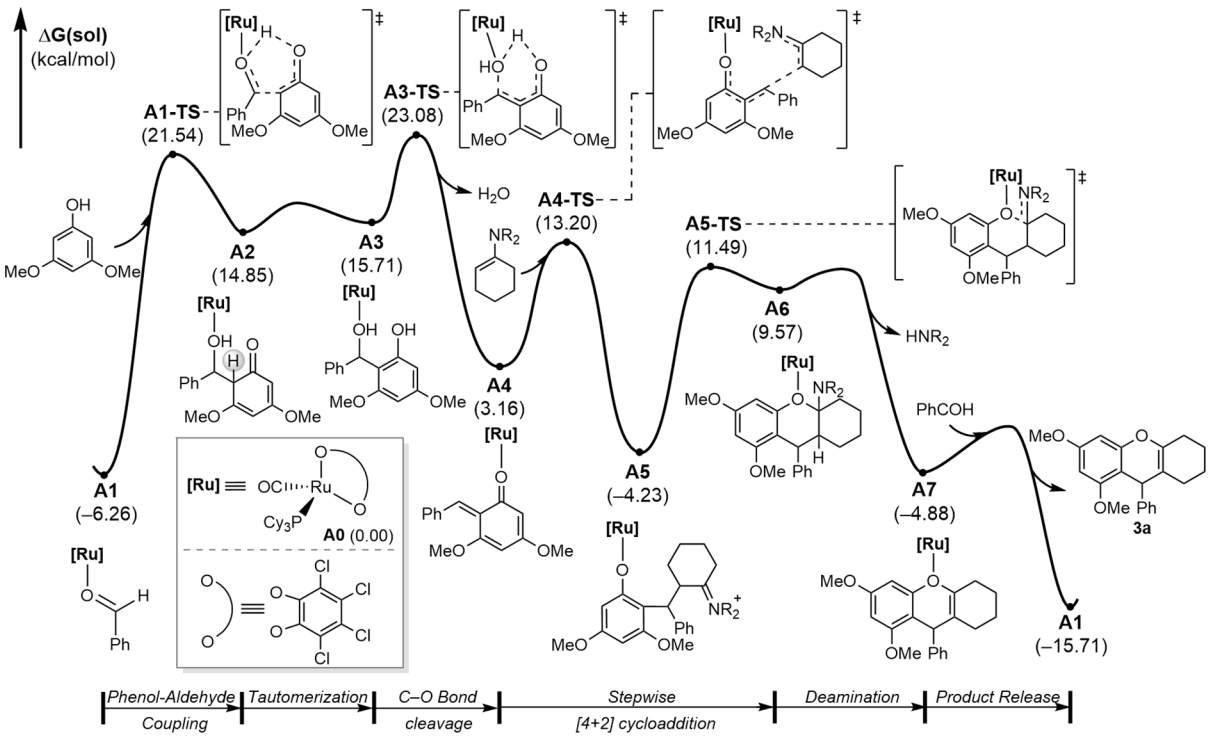

Figure 1. Computed energy profile for the coupling of 3,5-dimethoxyphenol with benzaldehyde and 4-(1-cyclohexen-1-yl)morpholine (NR_2 = *N*-morpholinyl).

synthon for the deaminative coupling reaction to form bicyclic 1,5-oxacin products.

We employed a number of biologically active steroidal ketone substrates for the multicomponent coupling reaction to further demonstrate its synthetic utility (Table 5). In this case, the enamine substrate was initially generated *in situ* from the treatment of 5α-pregnane-3,20-dione with morpholine, and the subsequent coupling reaction with 3,5-dimethoxyphenol and *para*-methoxybenzaldehyde was carried out under the standard conditions, which led to a highly diastereoselective formation of the xanthene product (+)-**3aa** (d.r. = 20:1). The coupling reaction was found to be highly chemoselective without affecting the other C17-acetyl group of the steroidal moiety. The colorless needles of (+)-**3aa** were grown in hexanes at room temperature, and their molecular structure was established by X-ray crystallography. The molecular structure of (−)-**3aa** showed an unusual orientation of the 17β-acetyl group with a large dihedral angle of C16-C17-C20-O2 = 151.1°. It should be noted that progesterone derivatives typically have an eclipsed conformation of the O2 carbonyl

https://doi.org/10.1021/acscatal.3c01651
ACS Catal. 2023, 13, 9051−9063

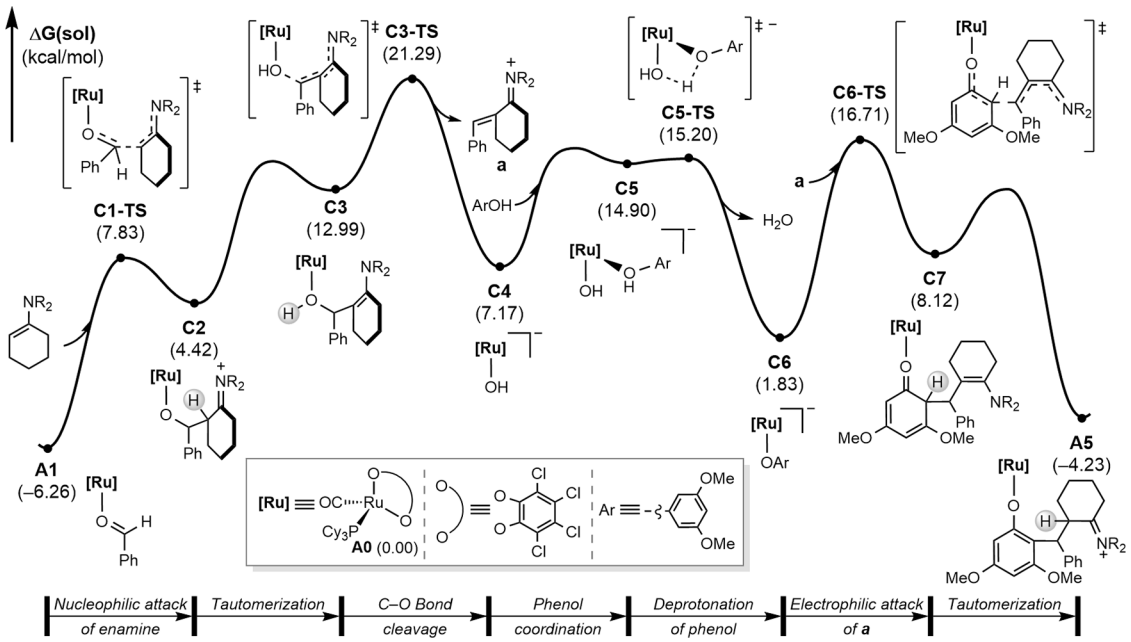

Figure 2. Computed energy profile for an alternate pathway starting from the reaction of benzaldehyde with 4-(1-cyclohexen-1-yl)morpholine (NR_2 = *N*-morpholinyl).

group with a relatively small dihedral angle of C16-C17-C20-O2 = 15°, and such an unusually large dihedral angle was observed only for the progesterone derivatives bearing 16α,17α-condensed 3-membered cyclic groups.[23] To validate the general trend of the diastereoselective formation of the products from steroidal derivatives, α-naphthol was reacted with 4-methoxybenzaldehyde, 5α-cholestan-3-one, and morpholine under the standard conditions, in which case also led to a highly diastereoselective formation of the xanthene product (−)-**3bb** (d.r. = 20:1). In contrast, the coupling reaction of 3,5-dimethoxyphenol with 2-hydroxybenzaldehyde and 5α-cholestan-3-one and 4-(1-cyclohexene-1-yl)morpholine led to the formation of a 1,3-dioxacin-steroidal derivative (+)-**5q**, with a modest 2:1 diastereomeric ratio. In this case, a modest diastereoselectivity may have resulted from unfavorable steric interaction between the phenoxy group (resulting from benzaldehyde) and C19 methyl group of the steroidal ketone substrate.

DFT Computational Study. To gain deep mechanistic insight into the coupling reaction, we conducted density functional theory (DFT) calculations for the coupling of 3,5-dimethoxyphenol with benzaldehyde and 4-(1-cyclohexen-1-yl)morpholine as representative substrates for the formation of the xanthene product **3**. The calculations were performed at the B3LYP-D3/cc-pVTZ(-f)|LACV3P//6-31G**|LACVP level of theory, and computational details can be found in the Supporting Information. We found the two most plausible mechanisms for the catalytic coupling reaction as delineated below out of several possible pathways that we initially probed as detailed in the Supporting Information.

In light of the previously established Ru-catecholate catalytic system that was formed from the reaction of a Ru−H complex with a 1,2-catechol ligand,[20] we assumed the Ru-catecholate complex **A0**, which would be formed *in situ* from the reaction of the Ru−H complex **1** with **L1**, as the catalytically active species for the coupling reaction (Figure 1). Previously, both experimental and computational studies on the dehydrative C−H coupling reaction of phenols with ketones showed that the presence of a Ru−H species is essential for promoting the *ortho*-arene C−H bond activation or for deprotonating hydroxyl group of the phenol substrate, as illustrated in Figure SS1.[21] However, in the current study, since the Ru-catecholate complex **A0** does not possess any Ru−H group, we found that the *ortho*-C−H arene activation pathways via either a concerted metalation-deprotonation (CMD) or a classical oxidative addition mechanism have the energy barrier well over 35 kcal/mol and thus are unlikely to occur under the operating experimental conditions at 110 °C (Figure SS2). Therefore, we searched for an alternative mechanistic pathway for the coupling reaction starting from **A0**.

The calculations quickly established that the coordination of the aldehyde substrate to **A0** leads to the formation of stable complex **A1**, which is 6.3 kcal/mol lower in energy relative to **A0**. The coupling reaction between phenol and aldehyde smoothly proceeds via **A1-TS** to produce **A2**. It is important to note that the proton transfer from phenol to the aldehyde carbonyl group and the C−C bond formation occur in a concerted manner. The coupling step turns the aldehyde substrate into an alcohol, while the phenol moiety becomes a dearomatized cyclohexadienone. This concerted reaction path via the transition state **A1-TS** allows one to bypass both CMD and oxidative addition mechanisms, as the direct *ortho*-C−H activation of phenol was not feasible with **A0**. Next, intermediate **A2** tautomerizes into phenolic intermediate **A3**, where the secondary alcohol undergoes heterolytic C−O bond cleavage via **A3-TS**. In this process, the electron on the C−O bond is rapidly transferred to the Ru−O bond, temporarily forming an anionic Ru−OH moiety. The phenolic proton of **A3** can be easily deprotonated, as it is situated in the vicinity of the Ru−OH moiety. This dehydration step leads to the formation of Ru-*o*-quinone methide species **A4**, which is anticipated to be the rate-determining step with an overall barrier of 29.3 kcal/mol from **A1**.

The resulting Ru-*o*-quinone methide **A4** undergoes a stepwise [4 + 2] cycloaddition with the enamine to form the xanthene scaffold. A highly electrophilic nature of the quinone

https://doi.org/10.1021/acscatal.3c01651
ACS Catal. 2023, 13, 9051−9063

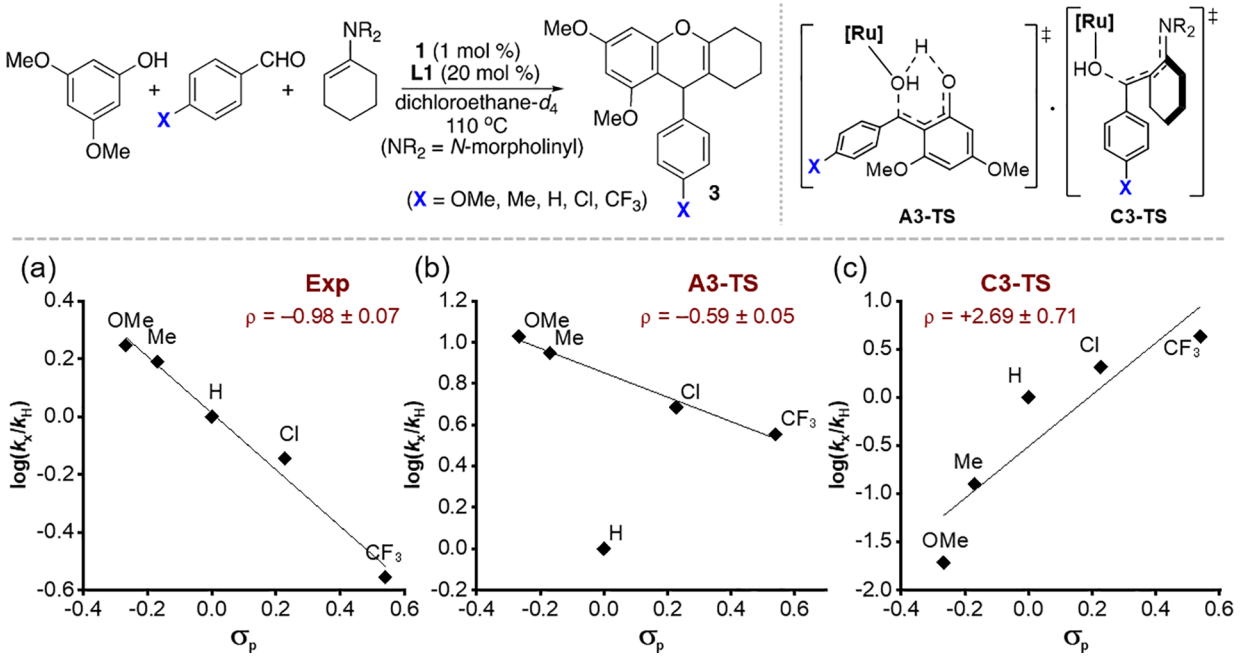

Figure 3. Hammett study from the reaction of 3,5-dimethoxyphenol, *p*-X-C_6H_4CHO and 4-(1-cyclohexen-1-yl)morpholine (X = OMe, Me, H, Cl, CF_3). (a) Experimental Hammett plot. Calculated rates are based on the difference between electronic energies for different reactants for the proposed rate-determining step via: (b) **A3-TS** and (c) **C3-TS**.

methide group facilitates the coupling reaction with the nucleophilic enamine to form transient iminium intermediate **A5**. The iminium group of **A5** promotes ring closure to form **A6** via **A5-TS** with an energy barrier of 15.7 kcal/mol. The subsequent deamination from **A6** is highly exergonic in forming the xanthene-coordinated **A7**, which readily releases the xanthene product **3a** from the ligand exchange with the aldehyde substrate along with regeneration of catalyst **A1**. Overall, the reaction from **A6** to **A1** releases a Gibbs free energy of 9.5 kcal/mol.

The mechanism discussed in Figure 1 features the coupling between aldehyde and phenol substrates in the first step, which is followed by the addition of an enamine in a later stage. A plausible alternative mechanistic path entails the coupling reaction of aldehyde first with enamine, and phenol is added at a later stage. We explored this possibility in detail and found that the energies encountered in this pathway are reasonable, as summarized in Figure 2. The coupling reaction is initiated by nucleophilic attack of enamine to the aldehyde through transition state **C1-TS**, generating iminium intermediate **C2**, which then tautomerizes to form Ru-enamine intermediate **C3**. The C−O bond of the secondary alcohol is cleaved via **C3-TS**, resulting in the formation of the iminium cation **a** and the anionic Ru-hydroxide **C4**. This step is expected to be rate-determining with an overall barrier of 27.6 kcal/mol from **A1**, which is slightly lower than the highest energy barrier for the reaction profile shown in Figure 1. The highly conjugated system of iminium ion **a** in a moderately polar solvent 1,2-dichloroethane will likely be stable as an ion-pair form. The coordination of the phenol substrate to **C4** forms the intermediate **C5**, and the subsequent deprotonation of the phenol yields the Ru-phenolate intermediate **C6**, traversing via **C5-TS** with a relatively low energy barrier of 8.1 kcal/mol. The anionic and highly nucleophilic Ru-phenolate group of **C6** readily reacts with an electrophilic iminium **a** to afford intermediate **C7**, which tautomerizes to form intermediate **A5**. The subsequent final steps leading to the product **3a** are identical to those illustrated in Figure 1.

Experimental and Computational Analyses on the Transition States. Since both mechanistic scenarios described above are chemically and energetically reasonable, we had not been able to decipher the operating mechanism on the basis of DFT-calculated data alone. We performed experimental Hammett studies to probe the electronic factors governing the rate-limiting step of the coupling reaction that could differentiate between the two plausible mechanisms. Thus, the rate of the coupling reaction of 3,5-dimethoxyphenol (0.20 mmol) with 4-(1-cyclohexen-1-yl)morpholine (0.20 mmol) and a series of *para*-substituted benzaldehydes *p*-X-C_6H_4CHO (0.20 mmol) (X = OMe, Me, H, Cl, CF_3) was measured by using NMR spectroscopy. The disappearance of the 3,5-dimethoxyphenol peak was normalized against an internal standard (hexamethylbenzene) in 30 min intervals, and the k_{obs} of each reaction was determined from a first-order plot of $-\ln([(3,5\text{-dimethoxyphenol})]_t/[(3,5\text{-dimethoxyphenol})_0])$ vs time. The Hammett plot was constructed from the correlation of $\log(k_X/k_H)$ versus σ_p, which showed a linear correlation pattern with a negative slope ($\rho = -0.98 \pm 0.1$) (Figure 3a).

To validate experimental Hammett data, we performed energy calculations for the coupling reaction with a series of *para*-substituted benzaldehyde derivatives and compared their energy differences resulting from the two transition states **A3-TS** and **C3-TS**. Interestingly, our DFT calculations revealed opposing trends for the two mechanisms considered. Figure 3b shows that the electronic energy of **A3-TS** increases as the benzaldehyde substrate becomes electron-poor, predicting that the fastest reaction rate with the lowest barrier would result for the methoxy-substituted benzaldehyde substrate, in agreement with the experimental Hammett data. On the other hand, the energy calculations via the transition state **C3-TS** showed the highest barrier for the methoxy-substituted benzaldehyde,

https://doi.org/10.1021/acscatal.3c01651
ACS Catal. 2023, 13, 9051−9063

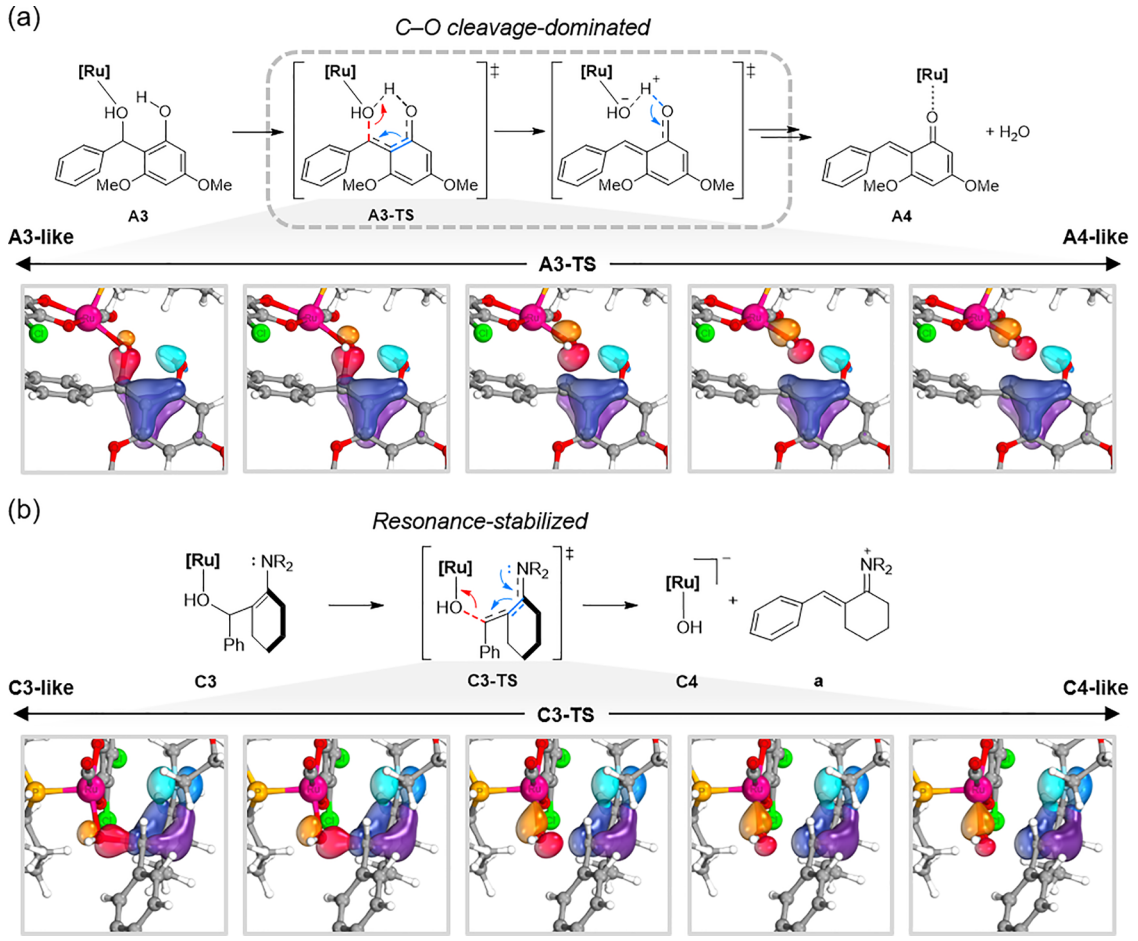

Figure 4. Comparison of the two transition states (a) **A3-TS** and (b) **C3-TS** from the reaction coordinate and the Intrinsic Bond Orbital (IBO) analysis (NR_2 = *N*-morpholinyl). The IBO plots are taken at steps ± 1.0, ± 0.6, and 0 along the intrinsic reaction coordinate.

indicating that the reaction rate would be the slowest for the methoxy-substituted benzaldehyde and the fastest for CF_3-substituted benzaldehyde (Figure 3c). Hence, an opposite Hammett correlation would be observed if **C3-TS** was involved for this reaction mechanism. Furthermore, the experimental Hammett slope (ρ = −0.98) corresponds to an energy difference of approximately 1.4 kcal/mol between the methoxy- and the trifluoromethyl-substituted benzaldehydes, which is consistent with the calculated energy difference of 0.8 kcal/mol for **A3-TS**. Notably, we believe that the benzaldehyde substrate case (X = H) is an outlier, possibly due to numerical calculation errors. Excluding the benzaldehyde case, the computed Hammett slope (ρ = −0.59) agrees reasonably well with the experimental value. Taken together, our experimental and computational results are consistent with the reaction pathway as depicted in Figure 1, with **A3-TS** as the rate-determining transition state.

To gain a deeper understanding of the unusual energy trends observed for **C3-TS** with electron-poor benzaldehyde derivatives, we examined the nature of both transition states in detail. In both **A3-TS** and **C3-TS**, the primary step involves C−O bond cleavage and transfer of the hydroxy group to the Ru center, as depicted in Figure 4. Conventional mechanistic intuition predicts that this bond should be cleaved heterolytically, generating a positive partial charge on the benzylic carbon and a negative charge on the hydroxyl-oxygen. As such, electron-donating groups at the *para*-position should stabilize the positive charge buildup and lower the barrier, as observed for **A3-TS**.

To better comprehend the origin of these unconventional energy trends, we analyzed the transformations occurring at both transition states in detail and discovered two electronic features that are significant, as schematically represented by the red and blue arrows in Figure 4. The first is the C−O bond cleavage, which we explained above, while the second involves π-resonance effects mediated by the enol and enamine moieties, respectively, resulting in a partial negative charge on the benzylic carbon, as shown in blue. The intrinsic bond orbital (IBO) analysis,[24] as shown in Figure 4, demonstrates that both electronic features are involved in the electronic process as the two transition states are traversed. **A3-TS** is the classical case where the C−O bond cleavage dominates, leading to increased positive charge polarization at the benzylic carbon at the transition state, resulting in classical Hammett behavior. In **C3-TS**, however, the π-resonance feature dominates and overrides the impact of the C−O bond cleavage as the amine functionality becomes formally an iminium group, characterized by a change of the NR_2 dihedral angle from 133° in **C3** to 177° in **C3-TS**. This places a negative partial charge on the benzylic carbon. This fundamentally different charge polarization reflects on the greater π-donor ability of the amine group compared to that of the hydroxyl group in **A3-TS**. As a result, the **C3-TS** transition state is stabilized by electron-withdrawing groups. As this

https://doi.org/10.1021/acscatal.3c01651
ACS Catal. 2023, 13, 9051−9063

Scheme 1. Proposed Mechanism of the Multicomponent C−H Coupling Reaction of 3,5-Methoxyphenol with an Aldehyde and a Cyclic Enamine

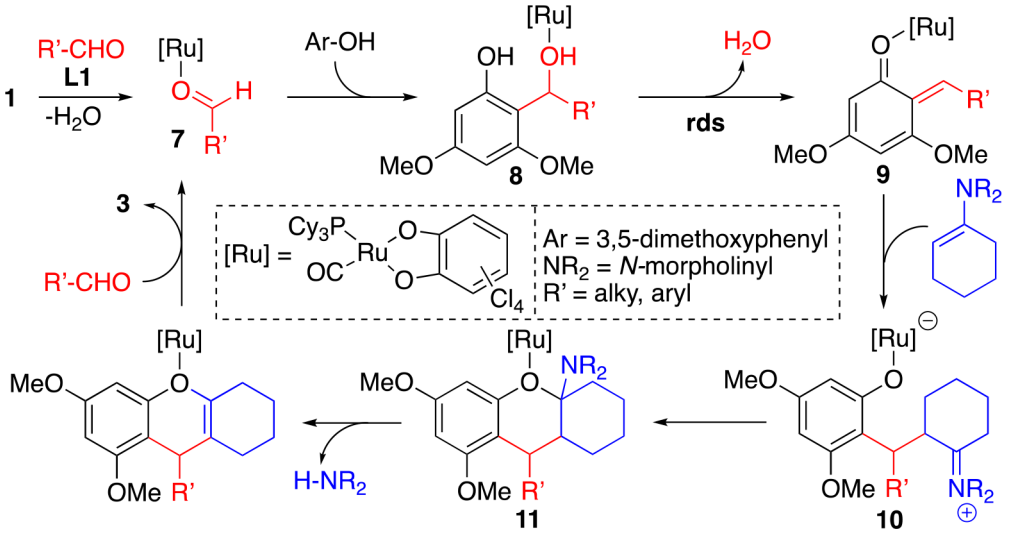

Hammett behavior is inconsistent with experimental observations, we can safely exclude the putative reaction pathway shown in Figure 2.

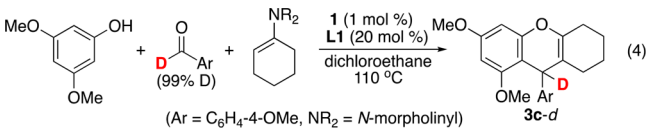

(4)

Deuterium Labeling Study. Another distinguishing feature between the two calculated mechanistic paths is the formation of the Ru−OH intermediate species **C4** as depicted in Figure 2. In the previously reported dehydrative coupling reaction of phenols with aldehydes,[21] we showed that the Ru−OH species can rapidly be converted into a Ru−H species especially in the presence of a hydrogen source such as water or 2-propanol and that the Ru−H species can effectively mediate rapid H/D exchange reaction at the *o*-quinone methide position. The DFT calculations established that such a hydride transfer step would be a reversible process, with the energy barrier of 15.9 kcal/mol (10.0 kcal/mol for the reverse reaction). The DFT calculations also predicted that an active Ru−OH or Ru−H catalytic intermediate species would mediate a reversible H/D exchange to the *o*-quinone methide position as illustrated in Figure SS2 (Supporting Information). To test the possibility of involvement of a Ru−OH or Ru−H species, we examined the possible H/D exchange process for the coupling reaction of 3,5-dimethoxyphenol, 4-methoxybenzaldehyde-α-d_1 (99.5% D), and 4-(1-cyclohexen-1-yl)-morpholine under the standard conditions (eq 4). The isolated product **3c**-*d* showed ca. 98% of deuterium on the methine position without any significant deuterium scrambling to other positions, as analyzed by ^{1}H and ^{2}H NMR spectroscopy, which clearly indicates that the aldehyde α-C−H bond was not broken during the coupling reaction (Figure S1, Supporting Information). The experimental result is consistent with the calculated mechanism, as shown in Figure 1, that does not involve any Ru−OH or Ru−H catalytic intermediate species.

Proposed Mechanism. We present a detailed mechanism of the multicomponent C−H coupling reaction of 3,5-methoxyphenol with benzaldehyde and an enamine on the basis of these experimental and computational results, as illustrated in Scheme 1. We propose that a catalytically active aldehyde-coordinated Ru(II)-catecholate complex **7** is initially generated from the reductive coupling reaction of **1** with the benzoquinone ligand **L1**. In support of this hypothesis, the Ru(II)-catecholate complex **4**, which was independently synthesized from the reaction of **1** with *t*-butyl-substituted 1,2-catechol and PCy_3 ligands, was found to be an active catalyst for the coupling reaction (Table 1, entry 9).[20] The deuterium labeling study also supports the idea that the active Ru catalyst should not contain any Ru−OH or Ru−H functionalities.

We initially considered two possible mechanistic sequences for the multicomponent coupling reaction starting from aldehyde-coordinated Ru-catecholate complex **7**. One possible pathway involves dehydrative coupling with phenol in the first step, which is followed by deaminative coupling with an enamine substrate (Figure 1). Alternatively, the aldehyde-coordinated Ru catalyst **7** would first undergo coupling with an enamine substrate, and dehydrative coupling with phenol would follow in subsequent steps (Figure 2). The DFT calculations showed that these two mechanistic pathways are energetically viable, and the magnitude of energy barrier for the rate-limiting step is quite similar for both pathways (29.3 vs 27.6 kcal/mol). To distinguish between these two possible pathways, we performed a Hammett study for the coupling reaction by using *para*-substituted benzaldehydes and compared its experimental data with the calculated energy values analyzed from the transition states **A3-TS** vs **C3-TS**. The calculated energy values obtained from **A3-TS** nicely correlated with the experimental Hammett data, where the coupling reaction is promoted by benzaldehyde substrates bearing an electron-releasing group (experimental $\rho = -0.98$ vs calculated $\rho = -0.59$). The IBO analysis on the two transition states **A3-TS** and **C3-TS** provided deeper insights into the electronic nature of the C−O bond cleavage process. Increasing positive charge polarization at the benzylic carbon is the dominant electronic factor leading to the transition state **A3-TS**, while π-resonance stabilization of the iminium ion overrides the charge polarization for **C3-TS**, which translates to an increase in a negative partial charge at the benzylic carbon during the C−O bond cleavage step. We excluded the

https://doi.org/10.1021/acscatal.3c01651
ACS Catal. 2023, 13, 9051−9063

putative reaction pathway via **C3-TS** since its electronic trend is opposite to the experimental Hammett data.

The combined DFT and experimental Hammett data support a mechanistic path, as illustrated in Figure 1 as the most likely operating mechanism. The DFT calculations provided a low-energy pathway where a nucleophilic addition of the *ortho*-arene carbon of phenol to the aldehyde-coordinated catalyst **7** leads to the formation of Ru-phenol complex **8**, which further proceeds with the dehydration reaction to form the dearomatized Ru-quinone species **9**. The DFT calculations also established that the dehydration step (C−O cleavage) is the rate-limiting step of the catalytic reaction, as indicated by its highest calculated energy barrier (29.3 kcal/mol). The subsequent nucleophilic addition of the enamine substrate to the vinyl carbon of the elaborated quinone group of **9** readily proceeds to form the zwitterionic Ru-aryloxo species with a pendent-armed iminium ion **10**. The final stage of the catalysis involves an intramolecular cyclization from **10** that is facilitated by the electrophilic iminium carbon to form the ruthenium-xanthene species **11**. The DFT calculations showed that the subsequent deamination and product-releasing steps are quite exergonic in forming xanthene product **3** along with regeneration of starting ruthenium catecholate complex **7**. Overall, the coupling reaction, which is exergonic by 9.5 kcal/mol, is driven by the formation of both water and amine byproducts.

CONCLUSIONS

In summary, we have successfully developed a Ru-catalyzed multicomponent deaminative C−H coupling method of phenols with aldehydes and enamines to install synthetically valuable xanthene and bicyclic dioxacin core structures in a step- and atom-efficient manner. The analogous coupling reaction of phenols with 2-hydroxyarylaldehydes and cyclic enamines selectively formed tricyclic 1,3-dioxacin derivatives. The combined experimental and DFT computational studies provided a detailed mechanistic portrait of the multicomponent coupling reaction, which features a sequential reaction process involving first the dehydrative C−H coupling of phenol with an aldehyde substrate, followed by the deaminative coupling with an enamine substrate. The catalytic coupling method employs readily available phenols, aldehydes, and amine substrates to efficiently assemble synthetically valuable oxygen heterocyclic core structures without using any reactive reagents or forming wasteful byproducts. Efforts to increase the synthetic applicability for this catalytic method are continuing in our laboratories.

EXPERIMENTAL SECTION

General Procedure for the Coupling Reaction of a Phenol with an Aldehyde and an Enamine. In a glovebox, a phenol (1.0 mmol), an aldehyde (1.0 mmol), an enamine (1.0 mmol), complex **1** (1 mol %) and **L1** (20 mol %) were dissolved in 1,2-dichloroethane (1 mL) in a 25 mL Schlenk tube equipped with a Teflon stopcock and a magnetic stirring bar. The tube was brought out of the glovebox, and it was stirred in an oil bath preset at 110 °C for 12 h. The reaction tube was taken out of the oil bath and cooled to room temperature. After the tube was open to air, the solution was filtered through a short silica gel column by eluting with CH_2Cl_2 (10 mL), and the filtrate was analyzed by gas chromatography-mass spectrometry (GC-MS). Analytically pure product **3** was isolated by column chromatography on silica gel (40−63 μm particle size, hexanes/EtOAc). The product was completely characterized by NMR and GC-MS spectroscopic methods.

Computational Method. All density functional theory (DFT) calculations were performed with the Jaguar 9.1 quantum chemistry program.[25] Electronic exchange and correlation energy contributions to the total electronic energy were approximated with B3LYP hybrid exchange functional along with Grimme's D3 dispersion correction (B3LYP-D3).[26] All intermediate and transition-state geometries were optimized with the 6-31G** basis set for main group atoms and LACVP basis set for Ru.[26,27] The LACVP basis set includes the Los Alamos relativistic effective core potentials (ECPs) for Ru atoms.[28] While these basis sets are adequate for obtaining accurate geometries, more reliable energies were obtained from the single-point calculations using Dunning's correlation-consistent triple-ζ basis set, cc-pVTZ(-f), for main group atoms and LACV3P** for Ru.[29] The zero-point energy (ZPE), entropic, and solvation contributions to the Gibbs energy are obtained from the same level of theory used in the geometry optimizations (B3LYP-D3/6-31G**/LACVP). The optimized geometries characterized as the local minima on the potential energy surfaces do not contain any imaginary frequency, whereas each of the transition states contains one imaginary frequency. The solvation free energy is computed as the difference between the energy of the optimized gas-phase structure and the energy inside a solvation shell of 1,2-dichloroethane in the form of a continuum dielectric(ε) equaling 10.3. The electronic energy in the solvation shell is calculated using the self-consistent reaction field (SCRF) method with a Poisson−Boltzmann solver. The overall scheme for obtaining approximate solution phase Gibbs free energies has been previously described.[30]

ASSOCIATED CONTENT

Supporting Information

The Supporting Information is available free of charge at https://pubs.acs.org/doi/10.1021/acscatal.3c01651.

Experimental procedures, characterization data for organic products, X-ray crystallographic data, Hammett study, deuterium labelling study (PDF)

DFT computational details, additional references, computed energies for optimized structures, vibrational frequencies for optimized structures (PDF)

Cartesian coordinates of all computed structures (XYZ)

X-ray crystallographic information of **3aa** (CIF)

X-ray crystallographic information of **3d** (CIF)

X-ray crystallographic information of **5a** (CIF)

X-ray crystallographic information of **5d** (CIF)

X-ray crystallographic information of **5p** (CIF)

X-ray crystallographic information of **6h** (CIF)

AUTHOR INFORMATION

Corresponding Authors

Mu-Hyun Baik − *Center for Catalytic Hydrocarbon Functionalizations, Institute for Basic Science (IBS), Daejeon 34141, Republic of Korea; Department of Chemistry, Korea Advanced Institute of Science and Technology (KAIST), Daejeon 34141, Republic of Korea;* orcid.org/0000-0002-8832-8187; Email: mbaik2805@kaist.ac.kr

https://doi.org/10.1021/acscatal.3c01651
ACS Catal. 2023, 13, 9051−9063

Chae S. Yi − *Department of Chemistry, Marquette University, Milwaukee 53233 Wisconsin, United States;* orcid.org/0000-0002-4504-1151; Email: chae.yi@marquette.edu

Authors

Nuwan Pannilawithana − *Department of Chemistry, Marquette University, Milwaukee 53233 Wisconsin, United States;* orcid.org/0000-0003-0148-7781

Mina Son − *Department of Chemistry, Korea Advanced Institute of Science and Technology (KAIST), Daejeon 34141, Republic of Korea; Center for Catalytic Hydrocarbon Functionalizations, Institute for Basic Science (IBS), Daejeon 34141, Republic of Korea;* orcid.org/0000-0001-5689-1648

Donghun Hwang − *Department of Chemistry, Korea Advanced Institute of Science and Technology (KAIST), Daejeon 34141, Republic of Korea; Center for Catalytic Hydrocarbon Functionalizations, Institute for Basic Science (IBS), Daejeon 34141, Republic of Korea*

Complete contact information is available at: https://pubs.acs.org/10.1021/acscatal.3c01651

Author Contributions

[||]These authors contributed equally.

Notes

The authors declare no competing financial interest.

■ ACKNOWLEDGMENTS

Financial support from the National Science of Foundation (CHE-2153885) is gratefully acknowledged. M.-H.B. is grateful for the financial support from the Institute for Basic Science (IBS-R10-A1). We thank Dr. Sergey Lindeman (Marquette University) for X-ray crystallographic analysis of the compounds listed in this article.

■ REFERENCES

(1) Recent reviews: (a) Ouyang, K.; Hao, W.; Zhang, W.-X.; Xi, Z. Transition-Metal-Catalyzed Cleavage of C−N Single Bonds. *Chem. Rev.* **2015**, *115*, 12045−12090. (b) Wang, Q.; Su, Y.; Li, L.; Huang, H. Transition-metal catalysed C−N bond activation. *Chem. Soc. Rev.* **2016**, *45*, 1257−1272. (c) Dander, J. E.; Garg, N. K. Breaking Amides using Nickel Catalysis. *ACS Catal.* **2017**, *7*, 1413−1423. (d) Shi, S.; Nolan, S. P.; Szostak, M. Well-Defined Palladium(II)-NHC Precatalysts for Cross-Coupling Reactions of Amides and Esters by Selective N−C/O−C Cleavage. *Acc. Chem. Res.* **2018**, *51*, 2589−2599.

(2) (a) Ruiz-Castillo, P.; Buchwald, S. L. Applications of Palladium-Catalyzed C−N Cross-Coupling Reactions. *Chem. Rev.* **2016**, *116*, 12564−12649. (b) Trowbridge, A.; Walton, S. M.; Gaunt, M. J. New Strategies for the Transition-Metal Catalyzed Synthesis of Aliphatic Amines. *Chem. Rev.* **2020**, *120*, 2613−2692.

(3) (a) He, F.-S.; Ye, S.; Wu, J. Recent Advances in Pyridinium Salts as Radical Reservoirs in Organic Synthesis. *ACS Catal.* **2019**, *9*, 8943−8960. (b) Garcia-Cárceles, J.; Bahou, K. A.; Bower, J. F. Recent Methodologies That Exploit Oxidative Addition of C−N Bonds to Transition Metals. *ACS Catal.* **2020**, *10*, 12738−12759.

(4) (a) Basch, C. H.; Liao, J.; Xu, J.; Piane, J. J.; Watson, M. P. Harnessing Alkyl Amines as Electrophiles for Nickel-Catalyzed Cross Couplings via C−N Bond Activation. *J. Am. Chem. Soc.* **2017**, *139*, 5313−5316. (b) Sun, S.-Z.; Romano, C.; Martin, R. Site-Selective Catalytic Deaminative Alkylation of Unactivated Olefins. *J. Am. Chem. Soc.* **2019**, *141*, 16197−16201. (c) Plunkett, S.; Basch, C. H.; Santana, S. O.; Watson, M. P. Harnessing Alkylpyridinium Salts as Electrophiles in Deaminative Alkyl-Alkyl Cross Couplings. *J. Am. Chem. Soc.* **2019**, *141*, 2257−2262. (e) Xu, J.; Bercher, O. P.; Talley, M. R.; Watson, M. P. Nickel-Catalyzed, Stereospecific C−C and C−B Cross-Couplings via C−N and C−O Bond Activation. *ACS Catal.* **2021**, *11*, 1604−1612.

(5) (a) Ni, S.; Li, C.-X.; Mao, Y.; Han, J.; Wang, Y.; Yan, H.; Pan, Y. Ni-catalyzed deaminative cross-electrophile coupling of Katritzky salts with halides via C−N bond activation. *Sci. Adv.* **2019**, *5*, eaaw9516. (b) Liu, Y.; Tao, X.; Mao, Y.; Yuan, X.; Qiu, J.; Kong, L.; Ni, S.; Guo, K.; Wang, Y.; Pan, Y. Electrochemical C−N bond activation for deaminative reductive coupling of Katritzky salts. *Nat. Commun.* **2021**, *12*, 6745.

(6) (a) Klauck, F. J.; James, M. J.; Glorius, F. Deaminative Strategy for the Visible-Light-Mediated Generation of Alkyl Radicals. *Angew. Chem., Int. Ed.* **2017**, *56*, 12336−12339. (b) Wu, J.; He, L.; Noble, A.; Aggarwal, V. K. Photoinduced Deaminative Borylation of Alkylamines. *J. Am. Chem. Soc.* **2018**, *140*, 10700−10704. (c) Lai, S.-Z.; Yang, Y.-M.; Xu, H.; Tang, Z.-Y.; Luo, Z. Photoinduced Deaminative Coupling of Alkylpyridium Salts with Terminal Arylalkynes. *J. Org. Chem.* **2020**, *85*, 15638−15644. (d) Yi, J.; Badir, S. O.; Kammer, L. M.; Ribagorda, M.; Molander, G. A. Deaminative Reductive Arylation Enabled by Nickel/Photoredox Dual Catalysis. *Org. Lett.* **2019**, *21*, 3346−3351. (e) Zhang, X.; Qi, D.; Jiao, C.; Liu, X.; Zhang, G. Nickel-catalyzed deaminative Sonogashira coupling of alkylpyridinium salts enabled by NN2 pincer ligand. *Nat. Commun.* **2021**, *12*, 4904.

(7) Fu, M.-C.; Shang, R.; Zhao, B.; Wang, B.; Fu, Y. Photocatalytic decarboxylative alkylations mediated by triphenylphosphine and sodium iodide. *Science* **2019**, *363*, 1429−1434.

(8) Sun, S.-Z.; Cai, Y.-M.; Zhang, D.-L.; Wang, J.-B.; Yao, H.-Q.; Rui, X.-Y.; Martin, R.; Shang, M. Enantioselective Deaminative Alkylation of Amino Acid Derivatives with Unactivated Olefins. *J. Am. Chem. Soc.* **2022**, *144*, 1130−1137.

(9) Crabtree, R. H. Deactivation in Homogeneous Transition Metal Catalysis: Causes, Avoidance, and Cure. *Chem. Rev.* **2015**, *115*, 127−150.

(10) (a) Si, T.; Kim, H. Y.; Oh, K. Substrate Promiscuity of *ortho*-Naphthoquinone Catalyst: Catalytic Aerobic Amine Oxidation Protocols to Deaminative Cross-Coupling and *N*-Nitrosation. *ACS Catal.* **2019**, *9*, 9216−9221. (b) Li, H.; Feng, H.; Zhang, J.; Van der Eycken, E. V.; Huang, L. Synthetic Access to Secondary Propargylamines via a Copper-Catalyzed Oxidative Deamination/Alkynylation Cascade. *J. Org. Chem.* **2019**, *84*, 10501−10508. (c) Thorve, P. R.; Maji, B. Deaminative Olefination of Methyl *N*-Heteroarenes by an Amine Oxidase Inspired Catalyst. *Org. Lett.* **2021**, *23*, 542−547. (d) Gao, Q.; Guo, Y.; Sun, Z.; He, X.; Gao, Y.; Fan, G.; Cao, P.; Fang, L.; Bai, S.; Jia, Y. Deaminative Cyclization of Tertiary Amines for the Synthesis of 2-Arylquinoline Derivatives with a Nonsubstituted Vinylene Fragment. *Org. Lett.* **2023**, *25*, 109−114.

(11) Zhao, X.; Liu, D.; Guo, H.; Liu, Y.; Zhang, W. C−N Bond Cleavage of Allylic Amines via Hydrogen Bond Activation with Alcohol Solvents in Pd-Catalyzed Allylic Alkylation of Carbonyl Compounds. *J. Am. Chem. Soc.* **2011**, *133*, 19354−19357.

(12) (a) Ashley, M. A.; Rovis, T. Photoredox-Catalyzed Deaminative Alkylation via C−N Bond Activation of Primary Amines. *J. Am. Chem. Soc.* **2020**, *142*, 18310−18316. (b) Dorsheimer, J. R.; Ashley, M. A.; Rovis, T. Dual Nickel/Photoredox-Catalyzed Deaminative Cross-Coupling of Sterically Hindered Primary Amines. *J. Am. Chem. Soc.* **2021**, *143*, 19294−19299.

(13) Recent reviews: (a) Wan, J.-P.; Gan, L.; Liu, Y. Transition metal-catalyzed C−H bond functionalization in multicomponent reactions: a tool toward molecular diversity. *Org. Biomol. Chem.* **2017**, *15*, 9031−9043. (b) Brandes, D. S.; Ellman, J. A. C−H bond activation and sequential addition to two different coupling partners: a versatile approach to molecular complexity. *Chem. Soc. Rev.* **2022**, *51*, 6738−6756.

(14) (a) Dongbang, S.; Confair, D. N.; Ellman, J. A. Rhodium-Catalyzed C−H Alkenylation/Electrocyclization Cascade Provides Dihydropyridines That Serve as Versatile Intermediates to Diverse Nitrogen Heterocycles. *Acc. Chem. Res.* **2021**, *54*, 1766−1778.

(15) Midya, S. P.; Sahoo, M. K.; Landge, V. G.; Rajamohanan, P. R.; Balaraman, E. Reversed reactivity of anilines with alkynes in the

rhodium-catalysed C−H activation/carbonylation tandem. *Nat. Commun.* **2015**, *6*, 8591.
(16) (a) Wang, X.-G.; Li, Y.; Liu, H.-C.; Zhang, B.-S.; Gou, X.-Y.; Wang, Q.; Ma, J.-W.; Liang, Y.-M. J. Three-Component Ruthenium-Catalyzed Direct *Meta*-Selective C−H Activation of Arenes: A New Approach to the Alkylarylation of Alkenes. *J. Am. Chem. Soc.* **2019**, *141*, 13914−13922. (b) Luan, Y.-Y.; Gou, X.-Y.; Shi, W.-Y.; Liu, H.-C.; Chen, X.; Liang, Y.-M. Three-Component Ruthenium-Catalyzed *meta*-C−H Alkylation of Phenol Derivatives. *Org. Lett.* **2022**, *24*, 1136−1140.
(17) (a) Jayakumar, J.; Parthasarathy, K.; Chen, Y.-H.; Lee, T.-H.; Chuang, S.-C.; Cheng, C.-H. One-Pot Synthesis of Highly Substituted Polyheteroaromatic Compounds by Rhodium(III)-Catalyzed Multiple C−H Activation and Annulation. *Angew. Chem., Int. Ed.* **2014**, *53*, 9889−9892. (b) Luo, C.-Z.; Jayakumar, J.; Gandeepan, P.; Wu, Y.-C.; Cheng, C.-H. Rhodium(III)-Catalyzed Vinylic C−H Activation: A Direct Route toward Pyridinium Salts. *Org. Lett.* **2015**, *17*, 924−927. (c) Pinkert, T.; Wegner, T.; Mondal, S.; Glorius, F. Intermolecular 1,4-Carboamination of Conjugated Dienes Enabled by Cp^*Rh^{III}-Catalyzed C−H Activation. *Angew. Chem., Int. Ed.* **2019**, *58*, 15041−15045. (d) Liang, Y.; Tan, Z.; Jiang, H.; Zhu, Z.; Zhang, M. Copper-Catalyzed Oxidative Multicomponent Annulation Reaction for Direct Synthesis of Quinazolinones via an Imine-Protection Strategy. *Org. Lett.* **2019**, *21*, 4725−4728. (e) Chen, Z.; Jin, S.; Jiang, W.; Zhu, F.; Chen, Y.; Zhao, Y. Multicomponent Synthesis of Iminocoumarins via Rhodium-Catalyzed C−H Bond Activation. *J. Org. Chem.* **2020**, *85*, 11006−11013. (f) Yu, S.; Hong, C.; Liu, Z.; Zhang, Y. Synthesis of Cyclopentenones through Rhodium-Catalyzed C−H Annulation of Acrylic Acids with Formaldehyde and Malonates. *Org. Lett.* **2021**, *23*, 5054−5059.
(18) Herraiz, A. G.; Cramer, N. Cobalt(III)-Catalyzed Diastereo- and Enantioselective Three-Component C−H Functionalization. *ACS Catal.* **2021**, *11*, 11938−11944.
(19) (a) Campbell, M. W.; Yuan, M.; Polites, V. C.; Gutierrez, O.; Molander, G. A. Photochemical C−H Activation Enables Nickel-Catalyzed Olefin Dicarbofunctionalization. *J. Am. Chem. Soc.* **2021**, *143*, 3901−3910. (b) Xu, S.; Chen, H.; Zhou, Z.; Kong, W. Three-Component Alkene Difunctionalization by Direct and Selective Activation of Aliphatic C−H Bonds. *Angew. Chem., Int. Ed.* **2021**, *60*, 7405−7411.
(20) (a) Arachchige, P. T. K.; Yi, C. S. Synthesis of Quinazoline and Quinazolinone Derivatives via Ligand-Promoted Ruthenium-Catalyzed Dehydrogenative and Deaminative Coupling Reaction of 2-Aminophenyl Ketones and 2-Aminobenzamides with Amines. *Org. Lett.* **2019**, *21*, 3337−3341. (b) Arachchige, P. T. K.; Handunneththige, S.; Talipov, M. R.; Kalutharage, N.; Yi, C. S. Scope and Mechanism of the Redox-Active 1,2-Benzoquinone Enabled Ruthenium-Catalyzed Deaminative α-Alkylation of Ketones with Amines. *ACS Catal.* **2021**, *11*, 13962−13972. (c) Gnyawali, K.; Arachchige, P. T. K.; Yi, C. S. Synthesis of Flavanone and Quinazolinone Derivatives from the Ruthenium-Catalyzed Deaminative Coupling Reaction of 2'-Hydroxyaryl Ketones and 2-Aminobenzamides with Simple Amines. *Org. Lett.* **2022**, *24*, 218−222.
(21) (a) Lee, H.; Mane, M. V.; Ryu, H.; Sahu, D.; Baik, M.-H.; Yi, C. S. Experimental and Computational Study of the (*Z*)-Selective Formation of Trisubstituted Olefins and Benzo-Fused Oxacycles from the Ruthenium-Catalyzed Dehydrative C−H Coupling of Phenols with Ketones. *J. Am. Chem. Soc.* **2018**, *140*, 10289−10296. (b) Pannilawithana, N.; Pudasaini, B.; Baik, M.-H.; Yi, C. S. Experimental and Computational Studies on the Ruthenium-Catalyzed Dehydrative C−H Coupling of Phenols with Aldehydes for the Synthesis of 2-Alkylphenol, Benzofuran and Xanthene Derivatives. *J. Am. Chem. Soc.* **2021**, *143*, 13428−13440.
(22) Liu, S.; Liang, J.; Zhang, P.; Li, Z.; Jiao, L.-Y.; Jia, W.; Ma, Y.; Szostak, M. Ruthenium-catalyzed divergent deaminative and denitrative C−N cleavages: facile access to quinoxalines. *Org. Chem. Front.* **2023**, *10*, 22−29.
(23) (a) Profeta, S., Jr.; Kollman, P. A.; Wolff, M. E. Conformation of the Progesterone Side Chain: Resolution of the Apparent Conflict between X-ray Data and Force-Field Calculations Using MM2. *J. Am. Chem. Soc.* **1982**, *104*, 3745−3747. (b) Lindeman, S. V.; Timofeeva, T. V.; Shklover, V. E.; Struchkov, Y. T.; Turuta, A. M.; Kamernitzky, A. V. The X-ray investigation of 16α,17α-thiazolidine derivatives of Δ4- and Δ5-pregnanes and conformational analysis of their oxathiolane analog. *Steroids* **1984**, *43*, 125−145.
(24) Knizia, G. Intrinsic Atomic Orbitals: An Unbiased Bridge between Quantum Theory and Chemical Concepts. *J. Chem. Theory Comput.* **2013**, *9*, 4834−4843.
(25) Bochevarov, A. D.; Harder, E.; Hughes, T. F.; Greenwood, J. R.; Braden, D. A.; Philipp, D. M.; Rinaldo, D.; Halls, M. D.; Zhang, J.; Friesner, R. A. Jaguar: A High-Performance Quantum Chemistry Software Program with Strengths in Life and Materials Sciences. *Int. J. Quantum Chem.* **2013**, *113*, 2110−2142.
(26) (a) Becke, A. D. Density-Functional Exchange-Energy Approximation with Correct Asymptotic Behavior. *Phys. Rev. A* **1988**, *38*, 3098−3100. (b) Lee, C.; Yang, W.; Parr, R. G. Development of the Colle-Salvetti Correlation-Energy Formula into a Functional of the Electron Density. *Phys. Rev. B* **1988**, *37*, 785−789. (c) Grimme, S.; Antony, J.; Ehrlich, S.; Krieg, H. A Consistent and Accurate Ab Initio Parametrization of Density Functional Dispersion Correction (DFT-D) for the 94 Elements H-Pu. *J. Chem. Phys.* **2010**, *132*, 154104. (d) Becke, A. D. Density-functional thermochemistry. III. The role of exact exchange. *J. Chem. Phys.* **1993**, *98*, 5648−5652. (e) Vosko, S. H.; Wilk, L.; Nusair, M. Accurate spin-dependent electron liquid correlation energies for local spin density calculations: a critical analysis. *Can. J. Phys.* **1980**, *58*, 1200−1211.
(27) (a) Ditchfield, R.; Hehre, W. J.; Pople, J. A. Self-Consistent Molecular-Orbital Methods. IX. An Extended Gaussian-Type Basis for Molecular-Orbital Studies of Organic Molecules. *J. Chem. Phys.* **1971**, *54*, 724−728. (b) Hehre, W. J.; Lathan, W. A. Self-Consistent Molecular Orbital Methods. XIV. An Extended Gaussian-Type Basis for Molecular Orbital Studies of Organic Molecules. Inclusion of Second Row Elements. *J. Chem. Phys.* **1972**, *56*, 5255−5257. (c) Rassolov, V. A.; Ratner, M. A.; Pople, J. A.; Redfern, P. C.; Curtiss, L. A. 6−31G* Basis Set for Third-Row Atoms. *J. Comput. Chem.* **2001**, *22*, 976−984.
(28) (a) Hay, P. J.; Wadt, W. R. Ab Initio Effective Core Potentials for Molecular Calculations. Potentials for the Transition Metal Atoms Sc to Hg. *J. Chem. Phys.* **1985**, *82*, 270−283. (b) Wadt, W. R.; Hay, P. J. Ab Initio Effective Core Potentials for Molecular Calculations. Potentials for Main Group Elements Na to Bi. *J. Chem. Phys.* **1985**, *82*, 284−298. (c) Hay, P. J.; Wadt, W. R. Ab Initio Effective Core Potentials for Molecular Calculations. Potentials for K to Au Including the Outermost Core Orbitals. *J. Chem. Phys.* **1985**, *82*, 299−310.
(29) (a) Dunning, T. H. Gaussian Basis Sets for Use in Correlated Molecular Calculations. I. The Atoms Boron through Neon and Hydrogen. *J. Chem. Phys.* **1989**, *90*, 1007−1023. (b) LACV3P: a triple-zeta contraction of the LACVP basis set developed by Schrodinger Inc.
(30) Ryu, H.; Park, J.; Kim, H. K.; Park, J. Y.; Kim, S.-T.; Baik, M.-H. Pitfalls in Computational Modeling of Chemical Reactions and How to Avoid them. *Organometallics* **2018**, *37*, 3228−3239.

https://doi.org/10.1021/acscatal.3c01651
ACS Catal. 2023, 13, 9051−9063